Pressure-Driven Sound Turbulence in a High-β Plasma

R. L. Stenzel
Department of Physics, University of California, Los Angeles, California 90024-1547
(Received 5 March 1990)

In a large laboratory plasma [1 m diam × 2 m, $n_e \leq 10^{12}$ cm^{-3}, $B_0 \simeq 15$ G, $\beta_e = nkT_e/(B_0^2/2\mu_0) \simeq 0.5$], strong density fluctuations ($\delta n/n \simeq 50\%$) near the lower hybrid frequency $(\omega_{ce}\omega_{ci})^{1/2}$ are identified as cross-field sound waves ($k_\perp \gg k_\parallel$, $\omega/k_\perp \simeq c_s$) driven unstable by the electron diamagnetic drift $\mathbf{v}_d = \nabla p \times \mathbf{B}/neB^2$, $v_d > c_s$. Wave steepening and refraction saturate the instability. Wave-enhanced transport but insignificant particle acceleration are observed.

PACS numbers: 52.35.Qz, 52.25.Fi, 52.35.Mw, 52.35.Ra

Low-frequency turbulence in magnetized plasmas is of fundamental interest in the areas of plasma waves, instabilities, transport, and heating. It plays an important role in space plasmas,[1,2] fusion plasmas,[3,4] and various laboratory plasmas.[5,6] The basic issues are the wave dynamics (instability, nonlinear saturation), the particle dynamics (acceleration, heating), and the modification of the fluid properties (anomalous transport). The present Letter addresses some of these issues in a particular parameter regime (magnetized electron fluid of significant $\beta_e \simeq 0.5$, unmagnetized ions) which has received attention in connection with magnetic shocks.[7,8] Here it is observed that the electron pressure gradient, rather than $\mathbf{E}\times\mathbf{B}$ drifts, generates strong cross-field sound turbulence. The dominant saturation mechanism is identified to be wave refraction by temperature gradients. Wave steepening leads to a wave-enhanced ion mass flow but negligible ion tail formation. Magnetic turbulence is associated with the wave diamagnetic currents.

The experiment is performed with a linear dc discharge in a uniform external magnetic field [Fig. 1(a)]. Diagnostics include Langmuir probes (n_e, kT_e, ϕ), magnetic probes $(\mathbf{B}_{(t)}, \mathbf{J})$, electric probes $(\mathbf{E} = -\nabla\phi - \partial\mathbf{A}/\partial t)$, and a directional particle energy analyzer.[9] The discharge is double pulsed [Fig. 1(b)] in order to observe wave growth and saturation with the second pulse fired in the afterglow of the first one. Data processing is performed with a digital oscilloscope used for noise-triggered (conditional) ensemble averaging.[10]

The basic plasma properties are summarized in Fig. 2. Radially, the density exhibits a strong gradient $(n/\nabla n \geq 20$ cm), the temperature has a weaker gradient $(T_e/\nabla T_e \geq 40$ cm), while the plasma potential gradients are negligible $(\mathbf{E} = -\nabla\phi_p \simeq 0)$ [Fig. 2(a)]. Axially, the plasma is highly uniform. The axial magnetic field inside the plasma B_p is smaller than the external field B_0 due to the electron diamagnetism [Fig. 2(b)]. Pressure balance $B_p^2/2\mu_0 + nkT_e \simeq B_0^2/2\mu_0 = \text{const}$ is approximately satisfied. The normalized electron pressure is $\beta_e = nkT_e/(B_0^2/2\mu_0) \simeq 0.5$. Ions are cold $(kT_i \leq 0.3$ eV) and essentially unmagnetized $(\omega_{ci}/2\pi \approx 300$ Hz $< \nu_i$, $r_{ci} \simeq 50$ cm $> v_i/\nu_i \simeq 10$ cm). The electron diamagnetic drift exceeds the sound speed $(v_{\text{dia}} = kT_e\nabla n/neB \simeq 10^6$ cm/sec $> c_s \simeq 2.4\times10^5$ cm/sec) as well as axial electron drifts $[(\nabla\times\mathbf{B})_z/\mu_0 ne \leq 2\times10^5$ cm/sec].

The basic features of the instability are shown in Fig. 3. The density fluctuations versus time [Fig. 3(a)] show a rapid growth and saturation upon turn-on of the discharge pulse. The fluctuations decay in the afterglow since pressure gradients decrease. The scaling of the fluctuation level with kT_e suggests that the instability is driven by electron pressure gradients. The frequency spectrum of the density fluctuations exhibits a peak at $f \simeq 40$ kHz, near but below the lower hybrid frequency, $f_{\text{lh}} = (f_{ce}f_{ci})^{1/2} \simeq 100$ kHz, and contain frequency components up to 1 MHz due to wave steepening. The peak

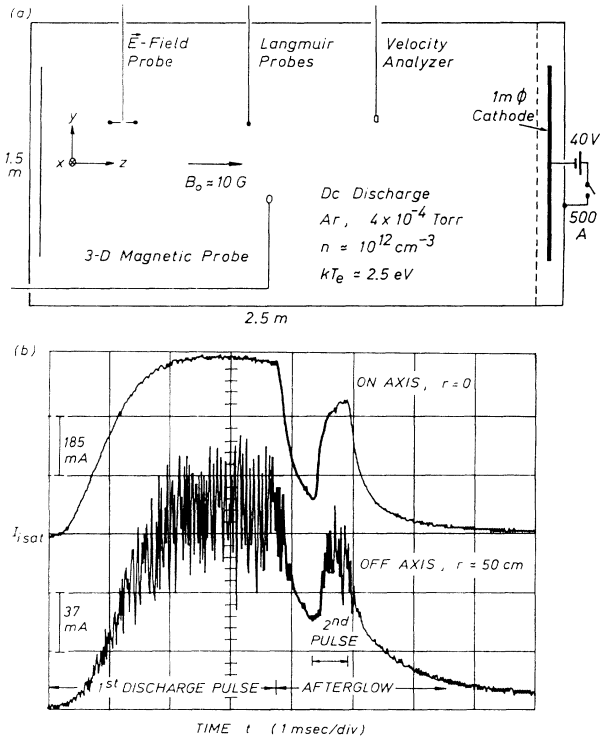

FIG. 1. (a) Schematic of the device. (b) Probe currents showing timing of experiment and density fluctuations investigated.

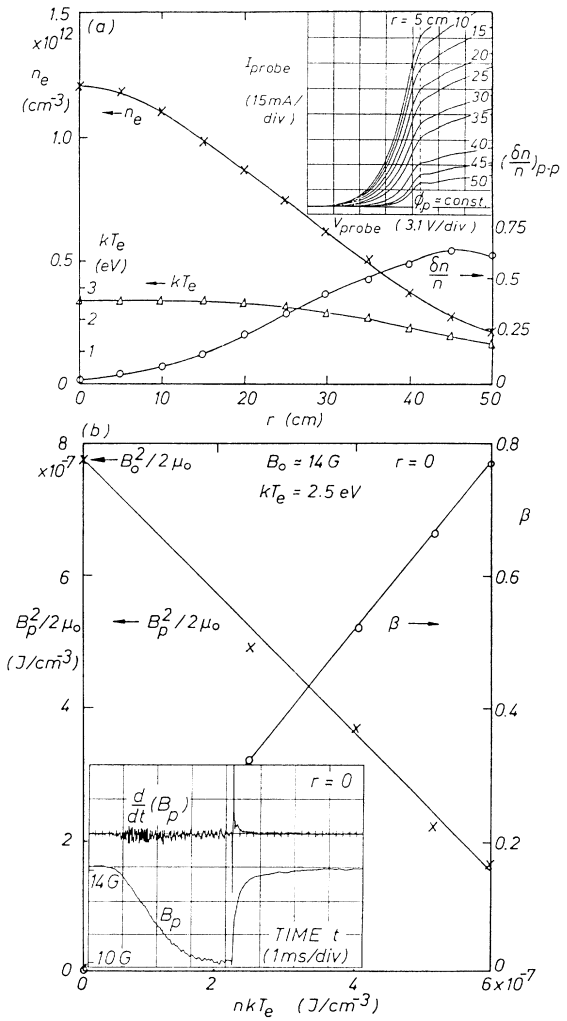

FIG. 2. Basic plasma properties. (a) Radial profiles of density, temperature, peak-to-peak fluctuations, and electric field $\mathbf{E} = -\nabla\phi_p \simeq 0$ obtained from Langmuir probe traces (see inset). (b) Plasma diamagnetism as obtained from magnetic probe traces (see inset).

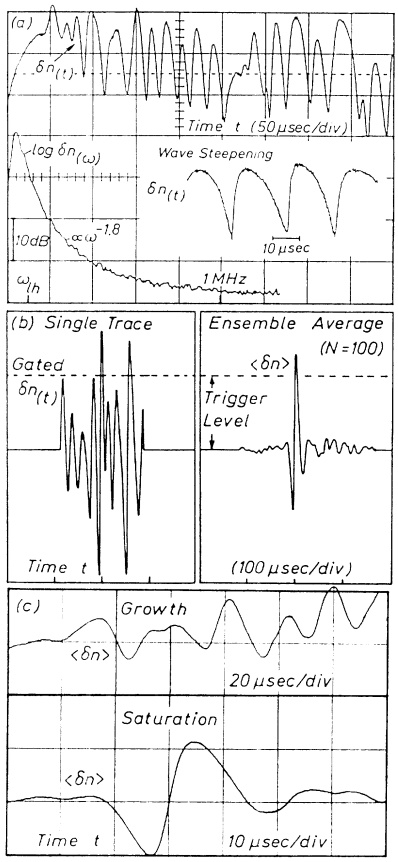

FIG. 3. Basic fluctuation properties. (a) Density fluctuations vs time showing growth and saturation. Frequency spectrum peaks below but near the lower hybrid frequency. Broad frequency spectrum is due to wave steepening. (b) Coherence properties obtained from noise-triggered ensemble averaging. Within a chosen time window (gate) the first fluctuation exceeding a given threshold value provides a trigger (timing and condition) to accept the wave form on an average over N repeated events. (c) Conditional averages showing long coherence times (wave trains) near instability onset and lack of temporal coherence (density clumps) in the saturated state.

frequency ($\sim 0.5 f_{lh}$) increases linearly with magnetic field ($10 < B_0 < 25$ G) and weakly decreases with density due to the diamagnetism.

The direction of wave propagation is obtained by a modified two-probe correlation technique [Fig. 3(b)]: Fluctuations from a fixed probe, gated by a broad time window during the stationary noise, are used to trigger a dual-channel digital oscilloscope at a desired fluctuation amplitude (typically $0.75\delta n_{max}$). The fluctuations from a second, movable probe are now ensemble averaged, which yields a nonzero mean value only for correlated signals. Thus, by locking the oscilloscope on a typical density fluctuation one can map its spatial and temporal coherence. Figure 3(c) shows examples of good temporal coherence during the linear growth (≥ 5 coherent oscillations) and poor coherence during saturation (~ 1 coherent oscillation).

Figure 4 displays the spatial properties of the saturated fluctuations. The average density perturbation $\langle \delta n \rangle$ propagates azimuthally in the direction of the electron diamagnetic drift [$v_{phase} < v_d$; Fig. 4(a)], and propagates radially outward with decreasing velocity [Fig. 4(b)]. Axially (not shown here), the fluctuations exhibit correlations to $\Delta z > 100$ cm and appear highly field aligned although the condition $k_\parallel/k_\perp \lesssim (m_e/m_i)^{1/2} = 3.7 \times 10^{-3}$ is difficult to establish in a high-β plasma. From two-dimensional correlation measurements, $\langle \delta n \rangle_{(x,y,t)}$, the average phase front is constructed [Fig. 4(c)]. The curved phase front is thought to be caused by refraction due to a radially varying phase velocity ($v_{ph} \simeq c_s \propto T_{e(r)}^{1/2}$). Near the onset of the instability the phase fronts are observed to be plane with $\mathbf{v}_{phase} \| \mathbf{v}_d$, but, in

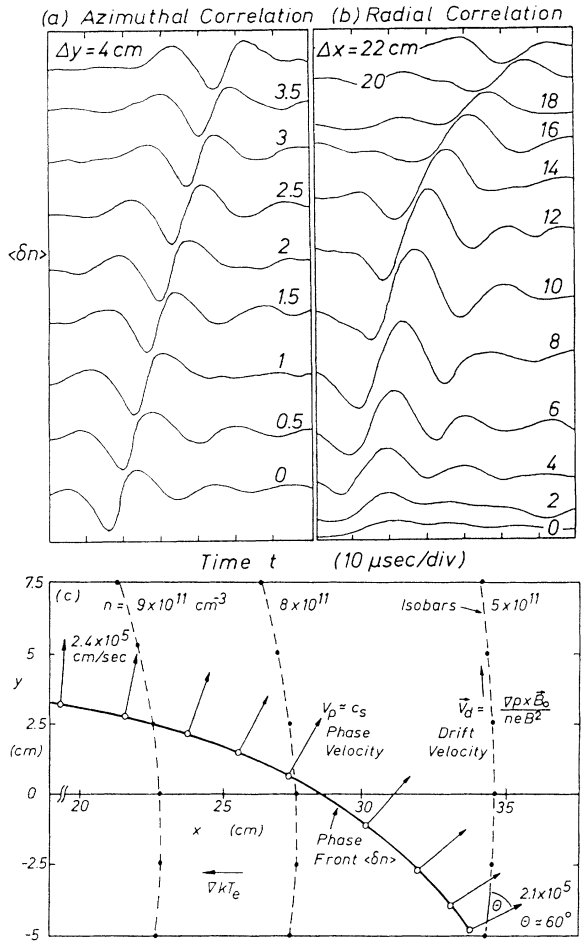

FIG. 4. Spatial properties of fluctuations. Conditional density averages vs time at different (a) azimuthal and (b) radial positions. (c) Typical two-dimensional phase front ($\partial/\partial z \simeq 0$) showing refraction of the sound wave by ∇kT_e which results in saturating the drift instability ($v_d \cos\theta \rightarrow c_s$).

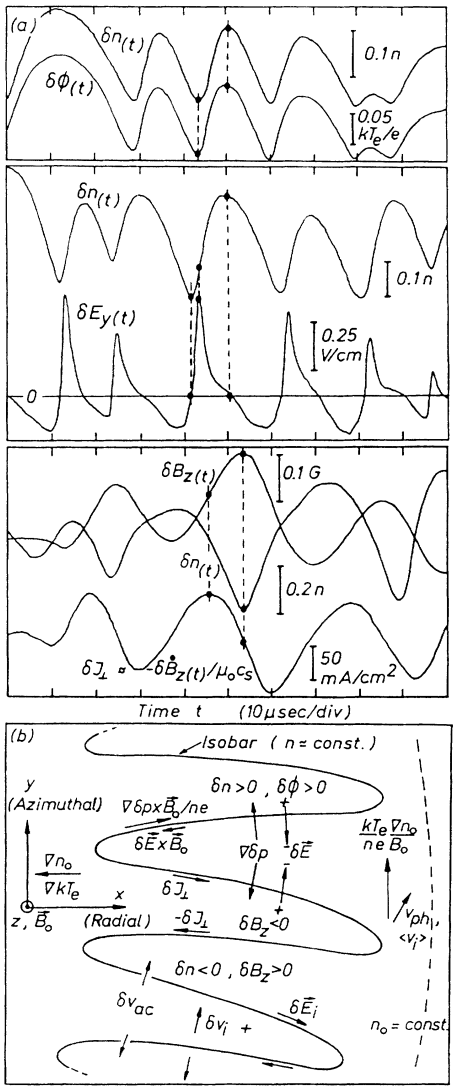

FIG. 5. (a) Correlation of fluctuations in density with those of potential, electric and magnetic fields, and currents. (b) Schematic view of microphysics within the fluctuations.

time, the waves refract into the shape shown in Fig. 4(c). The consequence of the refraction is a reduction in the growth rate since, following the curved wave ray, the drift no longer exceeds the azimuthal phase-velocity component of the wave ($v_d \leq \omega/k_y$). Waves that grow azimuthally refract radially, become marginally stable, and decay.

The density fluctuations have been correlated with other physical parameters such as potential and electric and magnetic fields. Single-shot, dual-channel traces [Fig. 5(a)] show a positive correlation between density and (floating) potential fluctuations from two field-aligned probes, consistent with the Boltzmann relation, although quantitatively $e\delta\phi/kT_e < \delta n/n$. Thus, there is a wave electric field $\delta\mathbf{E}_\perp = -\nabla_\perp \delta\phi$, which is observed directly with a differential dipole probe. The electrostatic field is large and spiky at the steepened wave fronts whose width approaches an electron Larmor radius. The wave $\delta\mathbf{E}\times\mathbf{B}$ drift is reduced by finite-Larmor-radius effects[11] and does not cancel the oppositely directed wave diamagnetic drift, $\nabla\delta p \times \mathbf{B}/neB^2$. The net electron drift is obtained from magnetic fluctuations δB_z which are observed to be anticorrelated with density fluctuations, consistent with pressure balance, but quantitatively $|\delta B_z/B_z| < (\beta/2)\delta n/n$. Since the observed time derivative $\delta\dot{B}_z$ represents a convective derivative,

$$(\partial/\partial t)\delta B_z = (\partial y/\partial t)(\partial/\partial y)\delta B_z \simeq -v_y \mu_0 J_x ,$$

the net current density $\delta J_\perp = nev_{d\perp}$ is obtained from the magnetic-loop signal $\delta J_\perp \simeq -\delta\dot{B}_z/c_s\mu_0$.

Figure 5(b) presents schematically the measured and derived quantities involved in the microphysics of the waves. The density perturbations create strong undula-

tions in the isobars since $\nabla\delta p > \nabla p$;

$$\frac{\nabla\delta n}{\nabla n} = \frac{\delta n}{n}\frac{n/\nabla n}{\delta n/\nabla\delta n} \approx 0.5\frac{20\text{ cm}}{1\text{ cm}} = 10.$$

Electron diamagnetic drifts are along the isobars and dominate over opposing $\delta\mathbf{E}\times\mathbf{B}$ drifts.

The time-varying wave electric field also gives rise to a small perpendicular ac electron drift, $\delta n_{ac\perp} = (\nu_{ei}/\nu_{ce}) \times \delta E_\perp/B$, dominated by Coulomb collisions ($\omega \ll \nu_{ei} \ll \nu_{ce}$). There is also a small ion inertial drift $\delta\mathbf{v}_i = e\mathbf{E}/m_i\omega$, which is negligible compared with the electron diamagnetic drift. The time-varying magnetic field creates an inductive electric field, $\delta E_i \simeq c_s\,\delta B_z$, which is negligible compared to the electrostatic field [$\delta E_i/\delta E \simeq \beta(m_e/m_i)^{1/2} \ll 1$]. Wave steepening creates a net ion flow $\langle v_i\rangle$ in the direction of wave propagation[11] which is observed from the average ion saturation current to a one-sided, rotated Langmuir probe. Hence, radial wave refraction causes an enhanced ion loss.

Particle acceleration and heating is often associated with strong lower hybrid waves[12] or electrostatic shocks.[13] Directional velocity analyzer traces, phase locked to fluctuations, have revealed negligible ion heating or tail formation. This is understood by the small fraction of resonant ions ($\mathbf{v}_i = \mathbf{v}_{phase}$) which lie in the velocity-space cone determined by the angular $\mathbf{k}$-vector spread [$2\pi(1-\cos\Delta\theta)/4\pi \ll 1$] and exceed sound speed [$\propto \mathrm{erfc}(c_s/v_{thi}) \ll 1$]. Since the electron pressure gradient ∇nkT_e is the source of the instability, global electron heating cannot be expected while local heating on expense of density profile modifications is theoretically possible but experimentally not observed. Thus, in the absence of significant wave-particle interactions the instability grows to large intensities [$(\delta B^2/2\mu_0)/nkT > 1\%$].

The author acknowledges helpful discussions with Dr. J. M. Urrutia. This work was supported by NSF Grants No. PHY87-13829 and No. ATM87-02793 and NASA Grant No. NAGW-1570.

[1]M. J. Keskinen and S. L. Ossakow, Radio Sci. **18**, 1077 (1983).
[2]H. L. Pecseli *et al.*, J. Geophys. Res. **94**, 5337 (1989).
[3]P. C. Liewer, Nucl. Fusion **25**, 543 (1985).
[4]J. D. Huba, J. F. Drake, and N. T. Gladd, Phys. Fluids **23**, 552 (1980).
[5]T. Huld *et al.*, Plasma Phys. Controlled Fusion **30**, 1297 (1988).
[6]A. Hirose *et al.*, Phys. Rev. Lett. **28**, 270 (1972).
[7]N. A. Krall and P. C. Liewer, Phys. Rev. A **4**, 2094 (1971).
[8]S. P. Gary, Plasma Phys. **15**, 399 (1973).
[9]R. L. Stenzel *et al.*, Rev. Sci. Instrum. **54**, 1302 (1983).
[10]H. Johnson *et al.*, Phys. Fluids **30**, 2239 (1987).
[11]F. F. Chen, *Introduction to Plasma Physics* (Plenum, New York, 1974), p. 34.
[12]J. F. Drake and T. T. Lee, Phys. Fluids **24**, 1115 (1981).
[13]R. J. Taylor *et al.*, Phys. Rev. Lett. **24**, 206 (1970).